Longitudinal Immune Monitoring Quantifies Disease Trajectory and Treatment Response in Graves' Orbitopathy

Ana Mendizabal-Sasieta*[,1], Laura Jiménez-Gracia*[,1], Umberto Perron[1], Marta Soto[1], Marta Grzelak[1], Pedro Bonifácio[1], Juan Luis Melero[1], Mariana Capelli[1], Roberta Vella Azzopardi[1], Holger Heyn[1]

1. Omniscope Inc., Delaware, United States of America

* These authors contributed equally.

Abstract

Background. Graves' disease (GD) is an autoimmune thyroid condition driven by thyroid-stimulating hormone receptor (TSHR) autoantibodies (TSI), frequently leading to hyperthyroidism and vision-threatening Graves' orbitopathy (GO) or Thyroid Eye Disease (TED). Despite its prevalence, the biological mechanisms driving disease onset, T-cell-mediated pathogenesis, and treatment resistance remain unclear. Because individual T-cell receptor (TCR) repertoires are highly private, cross-sectional snapshots often obscure these mechanistic and pathogenic signals. Longitudinal immune tracking overcomes this by using intra-individual baselines to track disease initiation, evolution, and therapeutic response.

Methods and Results. In a longitudinal tracking study, we followed a patient who developed dry eyes ~7 months postpartum, initially misdiagnosed as routine conjunctivitis. She was subsequently diagnosed with TSI-positive GD. Approximately 10 months later, she developed active, steroid-refractory GO/TED. Normalization of thyroid hormones with thiamazole failed to halt orbital disease progression. Subsequent high-dose pulse corticosteroid therapy failed to control ocular inflammation and induced elevated intraocular pressure. Switching to an anti-IL-6 receptor antagonist (tocilizumab) achieved rapid and complete clinical remission of orbital inflammation. Uniquely, peripheral blood mononuclear cells (PBMCs) had been banked across a 5-year window (2021-2026), enabling continuous longitudinal immune monitoring (osLifetime), spanning pre-onset to post-remission checkpoints.

Conclusion. osLifetime provided a real-time view of autoimmune T-cell activity. By monitoring the adaptive immune system across the entire clinical journey, it established a true pre-symptomatic baseline to benchmark disease progression and therapeutic transitions, capturing T-cell remodeling (manifesting as an acute drop in Immune Age alongside rising Inflammaging score), and even distinguishing corticosteroid failure from tocilizumab response. osLifetime turns complex immune dynamics into actionable quantitative signals, especially where routine biochemistry fails to reflect ongoing disease trajectory, paving the way for precision immunomonitoring in GO/TED and beyond.

Keywords. Graves' disease (GD); Graves' orbitopathy (GO); Thyroid Eye Disease (TED); T-cell receptor (TCR); osLifetime; Immune Age; longitudinal immune tracking.

Introduction

Graves' disease (GD) is the leading cause of an overactive thyroid (hyperthyroidism), affecting nearly 3% of women. It occurs when the immune system produces harmful autoantibodies that mistakenly lock onto the thyroid-stimulating hormone receptor (TSHR) [Lanzolla 2024; Antonelli 2020]. In up to 50% of patients, this manifests as Graves' orbitopathy (GO) or Thyroid Eye Disease (TED), where autoantibodies and autoreactive T cells target orbital fibroblasts through TSHR and IGF-1R cross-talk, driving an interleukin-6 (IL-6) inflammatory cascade [Lanzolla 2024; Fang 2021; Kim 2024].

While T cells are central to GD pathogenesis [Antonelli 2020; Fang 2021], their temporal dynamics remain poorly defined; we still know little about when pathogenic T cells first emerge, their correlation with antibody titers, and how quickly they respond to treatment. Previous studies on TCR repertoire rely on cross-sectional cohorts, taking single snapshots across different patients [Chen 2021; Jia 2022; Wang 2021; Liu 2024; Ke 2025; Zhou 2026]. However, because TCR repertoires are overwhelmingly private in nature (unique to an individual), inter-individual noise masks subtle auto-reactive signals [Wang 2020; Wang 2021].

Here, we present a 5-year longitudinal study (2021-2026) of a Hispanic woman tracking through pre-disease baseline, GD onset, corticosteroid-resistant Graves' orbitopathy (GO/TED), targeted anti-IL-6R biologic therapy, treatment withdrawal flare, and sustained remission. Because she was enrolled in a longitudinal immune-tracking program (osLifetime) before her symptoms began, her case captured multiple timepoints through full recovery. Using the osLifetime platform (combining Immune Age with Inflammaging and Senescence scores; Fig. S1) alongside comprehensive serial standard blood panels, we demonstrate how intra-individual immune tracking captures active autoimmune evolution where standard biochemistry falls short.

Results

Patient Information, Clinical Symptomatology and Diagnostic

A woman of mixed European and Indigenous American ancestry in her late 30s (1.64 m, 52 kg, BMI: 19.3 kg/m²) presented with a 3-week history of severe bilateral ocular burning, dryness, and discomfort. Her medical history was notable for a former history of light tobacco use (~5 cigarettes/day), which she discontinued upon becoming pregnant in February 2023, followed by an uncomplicated full-term pregnancy and delivery in November 2023. The ocular symptoms began in June 2024 (7 months postpartum) while actively lactating. She had no prior history of thyroid disease or ophthalmologic disorders. The patient's family history revealed maternal-line autoimmune disorders and thyroid dysfunction (Fig. S2).

Upon detailed retrospective review, the patient exhibited systemic thyrotoxic symptoms dating back to early 2024 (~2-3 months postpartum), including resting tachycardia, weight loss, polyphagia with nocturnal awakenings, telogen effluvium (hair shedding), and fatigue. These hyperthyroid features had been previously misattributed to typical postpartum stress and nursing demands, delaying her endocrinologic evaluation until after the onset of her ocular symptoms.

In July 2024, after receiving three prior misdiagnoses of routine viral conjunctivitis, she was evaluated by an ocular surface specialist who identified severe aqueous-deficient dry eye evidenced by a markedly abnormal ocular-surface hydration score (Schirmer test: 0 mm/5 min bilaterally; normal: >10 mm/5 min). Additionally, she demonstrated superior limbic keratoconjunctivitis (SLK), bilateral pigment dispersion, and axial myopia (Fig. S3). Subsequent endocrinologic evaluation confirmed previously unrecognized hyperthyroidism, and serologic testing established a diagnosis of Graves' disease (GD). Notably, at initial diagnosis, the severe ocular surface disease presented in isolation, without overt clinical signs of orbital involvement.

In February 2025, the patient resumed smoking (~3 cigarettes/day). Three months later, in May 2025 (10 months after her initial presentation of dry eye), she developed active, moderate-to-severe Graves' orbitopathy (GO) / Thyroid Eye Disease (TED), at which point she permanently quit smoking. She presented with bilateral periorbital and eyelid edema, conjunctival hyperemia, marked proptosis, retrobulbar pain, and progressive extraocular muscle dysfunction causing diplopia (Clinical Activity Score, CAS: 3/7) (Fig. S3). Optic nerve function remained preserved, as evidenced by intact color vision, normal visual acuity, and an unremarkable fundoscopic exam, ruling out dysthyroid optic neuropathy (DON).

Patient Longitudinal Profiling and Monitoring

Long before symptom onset, the patient was enrolled in the osLifetime longitudinal immune tracking program. We monitored her disease trajectory across ten strategic timepoints from 2021 to 2026 (t0-t9; Table 1), spanning pre-symptomatic baseline, acute onset, multiple therapeutic interventions, and clinical recovery. To complement her frequent routine clinical serology, osLifetime provided parallel multi-omic, immune profiling, using both co-sampled blood draws and event-driven checkpoints at key clinical inflections, to track systemic biological aging (Immune Age), immune cell activity (Inflammaging and Senescence) alongside autoantibody and clinical trends (Fig. 1, S1).

PHASE 1: PRE-SYMPTOMATIC BASELINE

Enrolled in the osLifetime program long before her first clinical symptoms emerged, her first osLifetime sample (t0; October 2021) served as a pre-disease baseline. Throughout her baseline period, she maintained completely normal blood panels, showing no alterations in thyroid function, hematology, or lipid metabolism. A couple of years later, during her pregnancy, routine thyroid serology remained within normal limits.

During the pre-symptomatic phase (2021-2023), the predicted Immune Age baseline was 37.9 years at t0 (October 2021; chronological age 36.0, Δ = +1.9) and 38.4 years at t1 (May 2023; chronological age 37.6, Δ = +0.8). Across these baseline measurements (t0 and t1), underlying

systemic Inflammaging scores were 0.694 (z = -2.786) and 0.738 (z = -1.490), while Senescence scores remained stable at 0.786 (z = -0.826) and 0.785 (z = -0.920), respectively. Importantly, both score trajectories remained below the population 90th percentile, and the modest elevation of Immune Age relative to chronological age falls well within normal physiological variance, reflecting a stable baseline with no clinically alarming signals.

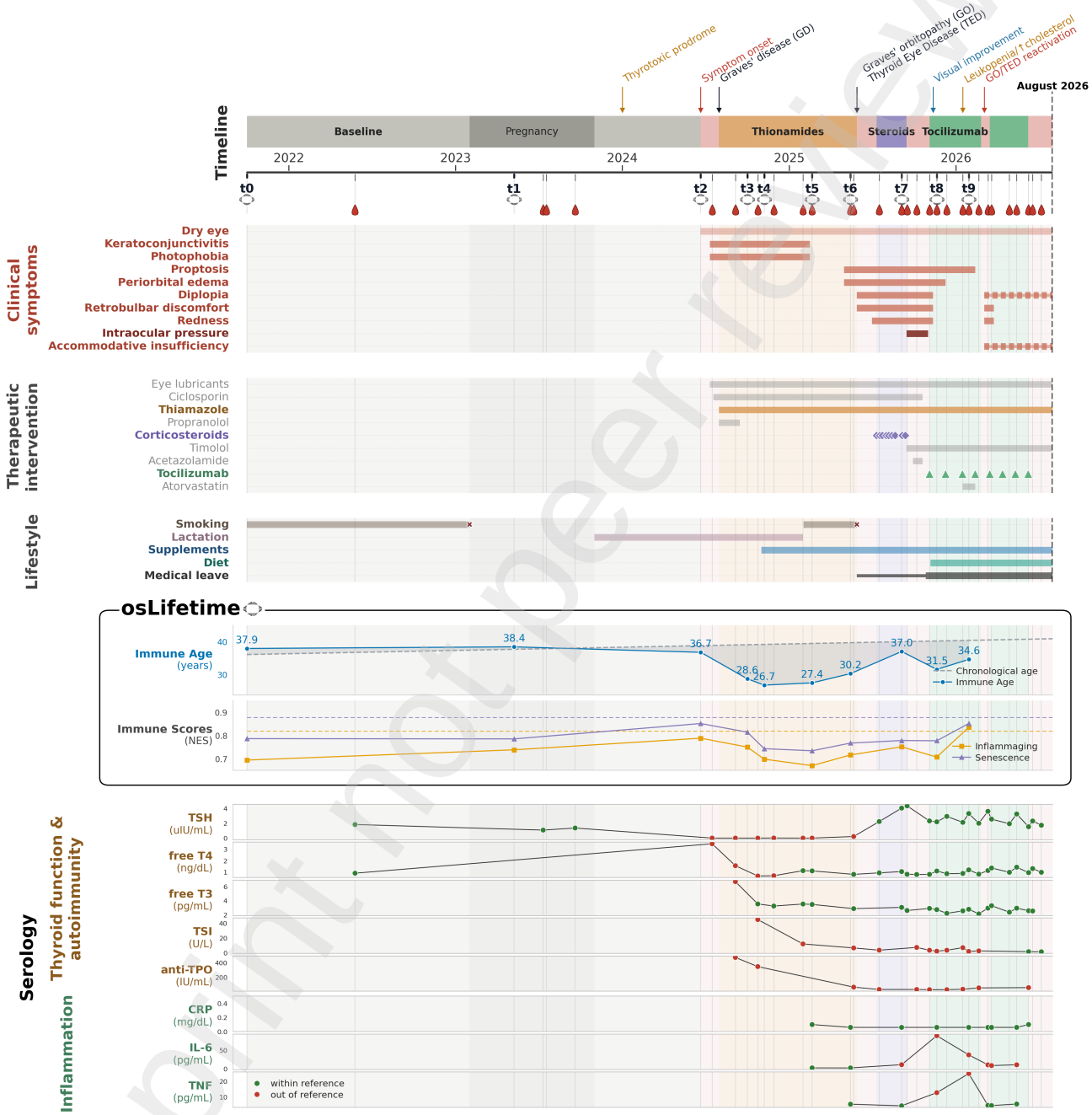

Figure 1. Longitudinal clinical timeline, therapeutic regimens, osLifetime immunodynamics and serology panels. (**Top**) Clinical timeline showing baseline, pregnancy, disease milestones (thyrotoxic prodrome, Graves' disease diagnosis, Graves' orbiopathy/TED onset, and reactivation), major treatment phases (thionamides, steroids, tocilizumab), and lifestyle factors. Timepoints t0-t9, indicate osLifetime sampling; blood icons indicate routine clinical laboratory panels (**Middle**) osLifetime immune profiling showing Immune Age relative to chronological age, with the grey shaded band marking the gap (acceleration/deceleration) between the two, alongside systemic Inflammaging and Senescence scores (Normalized Enrichment Score [NES]) over time, with dashed lines indicating the 90th percentile threshold (P90) of a reference population. (**Bottom**) Routine serology panels, detailing thyroid

function and autoantibodies (TSH, FT4, FT3, TSI/TRAb, anti-TPO) and systemic inflammatory markers (CRP, IL-6, TNF-α). Data points are color-coded based on reference thresholds: green denotes values within the normal reference range; red denotes values outside reference limits.

PHASE 2: ACUTE ONSET & DIAGNOSIS

Following postpartum (t2; July 2024), the patient presented with dry eye symptoms and was diagnosed with acute hyperthyroidism secondary to Graves' disease (GD). Serologic evaluation confirmed overt biochemical thyrotoxicosis: characterized by suppressed TSH along with elevated free T4 and free T3 levels, and strongly positive circulating autoantibodies, including thyroid-stimulating immunoglobulin (TSI/TRAb) and anti-thyroid peroxidase (anti-TPO). Anti-thyroglobulin (anti-Tg) levels remained within normal limits.

At acute symptom onset (t2), osLifetime immune readouts began departing significantly from pre-symptomatic baselines. This phase was marked by a prominent initial spike in both Inflammaging and Senescence scores, reaching 0.788 (z = +0.147) and 0.851 (z = +0.527), respectively. This coincided with the start of a shift in predicted Immune Age, which dropped to 36.7 years (chronological age 38.8), where the Δ inverted to -2.1 years before progressively decreasing further. Interestingly, osLifetime profiling revealed a distinct molecular lead time characterized by a progressive decrease in Immune Age coupled with an increase in systemic inflammation. Together, these signals alert from an unmanaged restructuring of the adaptive immune system (specifically the T-cell pool), which can be associated with an ongoing subclinical condition under subclinical autoimmune drive [Qi 2014], prior to symptomatic and clinical onset.

PHASE 3: THERAPEUTIC INTERVENTION & DYNAMIC TREATMENT TRACKING

First-Line Antithyroid Drug Therapy (ATD): Thiamazole

Following diagnosis, a stepped therapeutic strategy was implemented per ATA/EUGOGO guidelines [Ross 2016; Bartalena 2021] to control thyrotoxicosis and manage early dry eye disease. ATD therapy was initiated with Thiamazole (Tirodril; 20 mg/day starting July 2024, tapered to 2.5 mg/day over ~14 months), supplemented with a brief block-and-replace interval (adding levothyroxine/Eutirox 25 µg), propranolol for symptomatic adrenergic control, supportive ocular surface lubrication, and the subsequent supplementation with selenium and vitamin D.

This initial ATD regimen successfully normalized circulating free T3 and T4 levels, although TSH remained suppressed below optimal physiological limits. Serum autoantibody titers declined markedly from their peak (TSI ~45 in late 2024 falling to 6.6 by May 2025) yet remained persistently positive far above normal thresholds, highlighting a clear clinical dissociation between normalized thyroid hormone status and ongoing autoimmune drive [Hoang 2022; Lanzolla 2024].

Concurrently, serial osLifetime immune profiling revealed that Immune Age underwent a sharp, continuous decline, dropping down to 28.6 years (t3, October 2024; chronological age 39.0, Δ = -10.4), and reaching a minimum predicted age of 26.7 years (t4, November 2024; Δ = -12.4), before stabilizing at 27.4 years (t5, February 2025; Δ = -12.0). Crucially, this sustained drop during an acute flare does not represent biological rejuvenation or improved health, but rather a

deep restructuring of the systemic T-cell pool under chronic autoimmune drive. In contrast, the Inflammaging and Senescence scores functioned as acute indicators. Following the initiation of Thiamazole, both scores dropped rapidly to their lowest negative troughs at t5, with the Inflammaging score reaching 0.670 (z = -3.706) and the Senescence score reaching 0.734 (z = -2.058), before rebounding.

Despite achieving partial endocrine stabilization, ATD therapy failed to halt progressive orbital inflammation. Approximately 10-11 months after the initial GD diagnosis (May 2025; t6), the patient experienced the clinical emergence and rapid aggravation of active, moderate-to-severe Graves' orbitopathy / Thyroid Eye Disease (GO/TED), manifesting as bilateral periorbital and eyelid edema, conjunctival hyperemia, marked proptosis, retrobulbar pain, and diplopia [Ross 2016; Hoang 2022].

First-Line Immunosupressive Therapy: Intravenous Corticosteroid Pulse Therapy

With the clinical emergence of GO/TED, first-line immunosuppressive therapy was initiated using intravenous (IV) corticosteroids (Methylprednisolone) per the EUGOGO Kahaly regimen from July to September 2025 (500 mg weekly for 6 weeks, then 250 mg weekly for 6 weeks; intended cumulative dose: 4.5 g over 12 weeks) [Bartalena 2021]. During this therapeutic window, systemic endocrine serology remained stable: free T3 and free T4 remained close to normal limits, TSH returned to normal limits, and autoantibody titers (TSI/TRAb, anti-TPO) maintained a downward trend.

Upon initiating corticosteroids, osLifetime showed rapid stabilization of Inflammaging and Senescence scores. At t6 (May 2025), the Inflammaging score increased to 0.716 (z = -2.213) and Senescence to 0.767 (z = -1.322). By t7 (September 2025), they plateaued at moderate negative levels with an Inflammaging score of 0.751 (z = -1.063) and a Senescence score of 0.778 (z = -1.090), capturing the immediate, potent suppression of circulating cytokine cascades. Concurrently, Immune Age exhibited a steady, inertia-driven recovery; from a predicted age of 30.2 years at t6 (Δ = -9.5), it climbed back toward her chronological age (39.0), reaching 37.0 years (Δ = -3.0) at t7. This divergence highlights how sustained glucocorticoid administration allowed the underlying cellular repertoire to repopulate towards biological age, even while acute signatures remained suppressed.

Despite serological normalization, her orbitopathy demonstrated treatment refractoriness with no significant clinical improvement. Due to lack of ocular response, secondary elevation of intraocular pressure (IOP; managed with topical timolol and short-course oral acetazolamide), and steroid-induced cushingoid facial swelling, the final three scheduled infusions (doses 10-12) were cancelled in September 2025 [Bartalena 2021; Burch 2022].

Second-Line Targeted Biologic Therapy: Tocilizumab & Multimodal Support

Following corticosteroid failure, second-line targeted biologic therapy with tocilizumab (anti-IL-6 receptor monoclonal antibody; 8 mg/kg IV monthly for four consecutive doses) [Bartalena 2021; Pérez-Moreiras 2018, 2021] was initiated in November 2025. This was combined with a formal medical leave from work (starting October 2025) to eliminate screen exposure and psychological

stress, photobiomodulation (red-light) therapy, thermal-mask therapy to restore natural tear production, supportive lid-margin hygiene, preservative-free ocular lubrication, an anti-inflammatory diet, and the ongoing incorporation of L-carnitine, Omega-3 fatty acids, and calcium throughout the treatment course.

This multimodal strategy yielded dramatic clinical efficacy. The patient reported initial subjective visual improvement within ~8 days of the first infusion (November 12, 2025). Following two doses (December 2025), she noted an estimated ~80% reduction in periorbital edema and reduced diplopia frequency. By the fourth dose (February 2026), independent oculoplastic evaluation confirmed objective restoration of ocular motility and resolution of soft-tissue inflammation, leaving only minor residual sequelae. During this response phase, the patient noted that intermittent external environmental and lifestyle stressors (specifically air pollution, menstrual cycle transitions, sleep deprivation, acute psychological stress, alcohol consumption, and high-glycemic foods) correlated with transient exacerbations of ocular surface irritation and retrobulbar discomfort, highlighting the vulnerability of the ocular surface microenvironment to systemic inflammatory triggers.

Throughout biologic treatment, thyroid endocrine serology remained stable (normal free T3/T4, persistently positive TSI/TRAb and anti-TPO). Crucially, rapid orbital improvement occurred despite elevated TSI titers, confirming that therapeutic benefit tracked the localized orbital inflammatory axis rather than autoantibody clearance, a finding consistent with landmark *Tocilizumab GO clinical trials* [Pérez-Moreiras 2018, 2021].

Serial cytokine profiling revealed a classic pharmacodynamic signature of IL-6 receptor saturation: circulating serum IL-6 levels surged to a peak of ~90 pg/mL (vs. 1-2 pg/mL baseline) due to blockade of receptor clearance (direct confirmation of target engagement), followed by a secondary, delayed rise in TNF-α. Conversely, C-reactive protein (CRP) levels remained unreactive, reflecting direct inhibition of hepatic IL-6R/STAT3-dependent CRP synthesis. Expected pharmacodynamic side effects were noted in January 2026 [Pérez-Moreiras 2021], including mild leukopenia (reduced white blood cell count) coupled with hypercholesterolemia (elevated total and LDL cholesterol) (Fig. S4), managed with low-dose Atorvastatin (10 mg daily).

On osLifetime profiling, targeted IL-6 receptor blockade (t8, November 2025) caused the Inflammaging score to plummet to a secondary low of 0.707 (z = -2.509), accompanied by a parallel dip in Senescence to 0.777 (z = -1.097). This captures the real-time dampening of intracellular inflammatory signaling independent of elevated serum IL-6 or blunted CRP. Immune Age registered a transient downward shift to a predicted 31.5 years (chronological age 40.2, Δ = -8.7), reflecting clearance and cellular remodeling of IL-6-driven effector T-cell populations before resuming long-term recalibration. Interestingly, it was osLifetime readout that directly matched the rapid clinical resolution of active ocular symptoms, demonstrating osLifetime's ability to track the immediate dampening of downstream intracellular inflammatory cascades, bypassing both the artificial surge in circulating serum IL-6 and the physiologically blunted, unreactive CRP.

PHASE 4: TREATMENT SUSPENSION, FLARE & FULL REMISSION

To evaluate sustained clinical remission, a planned treatment suspension trial was initiated following the fourth dose (a one-month observation period agreed upon on February 25, 2026). Upon drug withdrawal, while thyroid endocrine serology panels remained stable, it led to a drop in serum cytokine levels, with circulating IL-6 settling at a 9-11 pg/mL plateau and TNF-α returning toward baseline physiological values.

Following a 1-month treatment pause in March 2026, the patient experienced a localized GO/TED reactivation characterized by the acute re-emergence of ocular redness, diplopia, and retrobulbar tightness. Notably, prior to peak clinical manifestation (t9, January 2026), while the patient was still receiving tocilizumab therapy, osLifetime profiling captured an ongoing increase in subclinical activity: Inflammaging and Senescence scores surged to positive peaks of 0.835 (z = +1.739) and 0.851 (z = +0.644), respectively, capturing active tissue re-inflammation in real time. Rather than signaling complete disease control, this rising trend reflected persistent, unresolved tissue inflammation under active therapy, demonstrating that the recovery was far from complete prior to the March treatment interruption. Simultaneously, Immune Age registered an upward shift to a predicted 34.6 years (chronological age 40.4, Δ = -5.8), indicating that systemic biological age starts showing ongoing immune landscape recalibration.

To regain inflammatory control, a second four-dose course of tocilizumab was initiated (March-June 2026) in anticipation of a second scheduled treatment suspension trial in July 2026. Upon re-initiating biologic therapy, the patient achieved sustained clinical remission with progressive re-establishment of physiological equilibrium. Ocular symptoms showed resolution of retrobulbar discomfort; however, the patient experiences persistent intermittent diplopia and accommodative insufficiency (difficulty focusing) attributed to chronic orbital tissue swelling secondary to prior inflammatory episodes. Definitive management will likely require surgical intervention (e.g., orbital decompression or corrective strabismus surgery), with supportive care currently consisting of mild aqueous dry eye with topical lubricants.

Endocrine serology in July 2026 demonstrated robust biochemical stability, with circulating free T3/T4 and TSH levels fully maintained within normal reference limits. Concurrently, circulating autoantibody titers showed marked improvement: by mid-2026, TSI/TRAb had normalized to physiological levels, while anti-TPO remained only modestly elevated and thyroglobulin (Tg) levels presented as notably elevated. This definitive stabilization of TSI, coinciding with localized orbital remission, is particularly notable given that TSI titers had remained persistently positive and fluctuant throughout the active disease phase and initial biologic course. From the same serological panel, circulating serum cytokine metrics (IL-6 and TNF-α) stabilized without secondary fluctuations, confirming predictable pharmacodynamic re-engagement, while systemic metabolic parameters following Atorvastatin co-therapy and completion of the second biologic course revealed slight elevations in total and LDL cholesterol, though atherogenic risk indices remained strictly within normal parameters (Fig. S4). These combined metrics remain under ongoing longitudinal evaluation as the patient enters her second treatment suspension trial.

Integrative Immunodynamics: Molecular mechanisms and systemic Immunity

To move beyond longitudinal cellular immune tracking into molecular mechanistic governing disease progression and therapeutic intervention, we performed feature-level deconstruction of TCR repertoires and transcriptomic profiles across all disease milestones (t0-t9).

DECONSTRUCTION OF LONGITUDINAL TCR REPERTOIRE DYNAMICS

To resolve structural shifts within the T-cell immune compartment across key disease milestones, we analyzed TCR repertoire dynamics and computationally inferred T-cell subset phenotypes (Δ CD4:CD8 ratio) alongside longitudinal clinical phases (Fig. 2). During pre-symptomatic homeostasis (t0), the patient maintained a polyclonally balanced repertoire (S = 0.516, clonality = 0.057, E_H = 0.627, D_{50} = 0.214) serving as a reference point for subsequent disease stages. Low dissimilarity between t0 and t1 (13% turnover) confirmed baseline stability, which was preserved through full-term pregnancy alongside a homeostatic CD4:CD8 ratio, reflecting peripheral tolerance and gestational immune regulation. The onset of Graves' Disease (t2-t3) marked a departure from homeostasis, characterized by contracting richness, reduced dominance and a drop in the CD4:CD8 ratio, driven by the acute peripheral depletion or tissue-homing of CD4+ helper and regulatory T-cell subsets to the thyroid gland [Nada & Hammouda 2014]. Anti-thyroid drug (ATD) initiation (t3) depressed richness alongside elevated clonality and reduced dominance. During ATD tapering, sequential turnover accelerated from 11% (t3-t4) up to 42% (t5-t6), unmasking a subclinical restructuring of the peripheral T-cell pool months before Thyroid Eye Disease (TED/GO) clinically manifested at t6.

Throughout this phase, the CD4:CD8 ratio remained depressed, reflecting CD4+ compartment contraction typical of active autoimmune thyroiditis [Nada & Hammouda 2014] and ATD treatment [Volpé 2001; Yang 2015], where thionamides continue to alter T-cell balance by suppressing peripheral helper pools or expanding cytotoxic compartments. High turnover (55%, t6-t7) persisted at TED onset. Intravenous corticosteroid pulse therapy (t7) drove broad bystander suppression, elevating clonality to its maximum peak (0.090), depressing richness (S = 0.438), and pushing D_{50} down to 0.149, while keeping the CD4:CD8 ratio suppressed [Maliah 2022], as systemic steroids preferentially depleted non-specific T cells while sparing corticosteroid-resistant pathogenic clones. Crucially, hyper-expanded T-cell clones surged to occupy >3.5% of the total repertoire space at t7, revealing the steroid refractoriness despite transient serological gains. Targeted anti-IL-6R blockade with tocilizumab (t8) successfully disrupted this pathogenic trajectory, prompting rapid clearance of hyper-expanded clones (<1.5% space), restoring dominance (D_{50} = 0.200), and recovering richness (S = 0.533). Tocilizumab also restored the CD4:CD8 ratio toward baseline [Tanaka 2011], likely mediated by blocking IL-6-driven Th17 differentiation and allowing for the reconstitution of the naive and regulatory CD4+ T-cell pools. During drug withdrawal (t9), persistent turnover (41%), a secondary uptick in top clone space (~1.8%), and CD4:CD8 ratio stabilization near baseline signaled ongoing adaptive immune modulation.

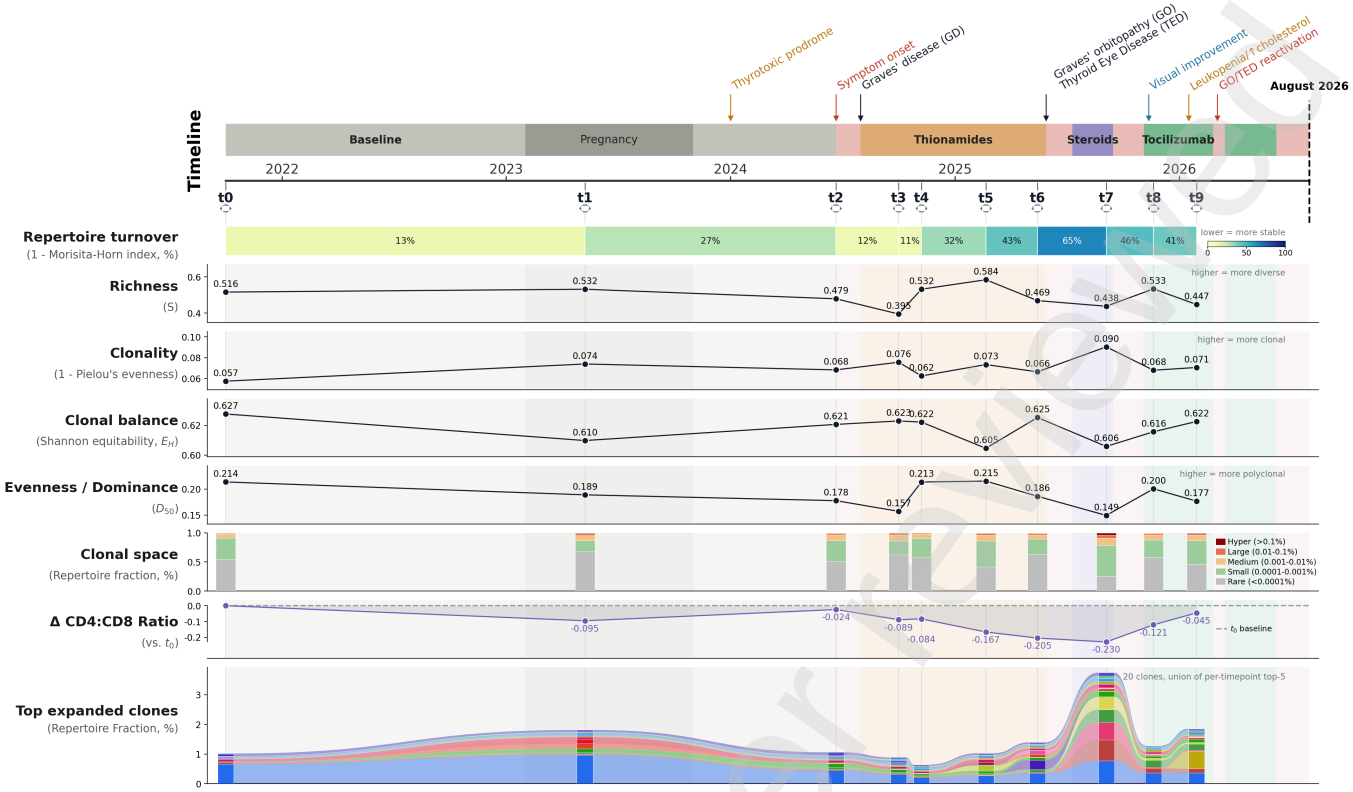

Figure 2. Longitudinal clinical timeline, therapeutic regimens, and deep T-cell receptor (TCR)-sequencing repertoire dynamics (osTCR). Overview of key disease milestones mapped alongside therapeutic phases (thionamides, steroids, tocilizumab) and osLifetime sampling intervals (t0-t9). **(Top)** Longitudinal TCR repertoire metrics: *Repertoire turnover* (sequential dissimilarity; lower values indicate greater stability); *Richness (S)* (count of unique clonotypes); *Clonality* (degree of oligoclonal focus); *Clonal balance* (Shannon equitability, E_H); *Evenness / Dominance* (D_{50}) (percentage of unique clonotypes accounting for 50% of sequencing reads); and *Clonal space* (fractional distribution across clone size classes ranging from rare to hyperexpanded). **(Middle)** Longitudinal deviation (Δ) in the computationally predicted CD4:CD8 T-cell ratio relative to the healthy baseline (t0). Dashed horizontal reference lines mark baseline values (t0, Δ = 0), with gray shaded areas highlighting the magnitude and direction of trajectory shifts (increases/decreases) across timepoints. **(Bottom)** Alluvial plot illustrating the cumulative TCR repertoire fraction (%) occupied over time by the dominant clonotypes (union of top-5 clones per-timepoint, *n* = 20 unique clones).

Because individual TCR repertoires are overwhelmingly private, cross-sectional analyses often struggle to isolate true pathogenic drivers from stochastic background noise [Wang 2021]. To address this, we obtained event-related (ER) clones by comparing longitudinal repertoires across defined sampling intervals anchored to specific clinical inflection points (Fig. S5a). Because Graves' TCR profiles are stage-dependent [Jia 2022; Chen 2021], each interval was matched to its expected signature and trajectory: clonal expansion at acute onset (t2-t3, Newly diagnosed disease (NGD)), at the emergence of refractory orbitopathy (t6-t7, refractory disease (RGD)) and across their progression (t3-t7, progression drivers (NGD-RGD)), and clonal contraction under effective biologic therapy (t7-t9) (see Methods). Acute GD onset (t2-t3) triggered a rapid wave of 6,247 significantly expanded clonotypes, the majority arising de novo (4,537 de novo vs 1,710 pre-existing at t2). The emergence of active orbitopathy (t6-t7) induced a larger oligoclonal surge of 7,656 expanded clonotypes (5,880 de novo, 1,776 pre-existing at t6). Their continued expansion through high-dose methylprednisolone pulses underscores the intrinsic resistance of these putatively pathogenic T cells to glucocorticoid-induced apoptosis. Targeted IL-6R blockade

(t7-t9) drove a profound, selective depletion of the disease-associated T-cell clones: statistical contraction modeling confirmed that 2,826 clonotypes underwent significant contraction or complete peripheral depletion (1,588 de novo, 1,238 pre-existing at t9). Notably, 2,155 of these (76% of the contracted set) had significantly expanded during the GO/TED flare (t6-t7), and the overlap was concentrated among the most-expanded clones.

To determine whether these adaptive responses were driven by specific structural T-cell receptor features, we performed V-J gene-usage enrichment analysis on the statistically significant ER clones (Fig. S5; see Methods, Gene-usage enrichment). While whole-repertoire V-J usage remained largely stable across the disease trajectory (Fig. S5b), isolating the differentially expanded and contracted ER clonotypes revealed event-specific gene-segment enrichments (Fig. S5c). At the clonotype level (counting how many event clones carry the disease architecture), the general GD-associated V-J compartment was significantly over-represented among expanded clones at every milestone, most strongly at acute onset (t2-t3; enrichment fold 2.05, $p < 10^{-23}$), with a distinct NGD signature emerging in the same interval (fold 1.34, $p < 10^{-3}$) and not thereafter. This clonotype-level enrichment was carried by a single dominant TRBV segment (TRBV12-3) and was shared between de novo emerging populations and pre-existing clones. Notably, no comparably restricted TRBJ pairing accompanied this V-segment bias. When weighted by abundance rather than unique clonotype count, RGD and progression-associated V-J pairings, which were not over-represented by clone count, were those that dominated the repertoire during the active GO/TED window (abundance fold ~1.7 and ~3.2, respectively), consistent with a small number of highly expanded pathogenic clones carrying the disease-associated architecture rather than a broad numerical expansion. Cross-testing the V-J architecture of contracted versus expanded ER clonotypes upon tocilizumab administration confirmed that IL-6R blockade selectively targeted this disease-enriched, high-abundance compartment, which showed the strongest depletion enrichment of the entire panel (contraction abundance fold up to 4.0). These dynamics show that the disease-associated repertoire can be followed as a longitudinal readout of disease activity and treatment response within a single patient.

TRANSCRIPTIONAL LANDSCAPES: UNRAVELING INFLAMMATORY CASCADES

To bridge systemic serum dynamics with granular cellular mechanisms and drug responses, we performed feature-level deconstruction of peripheral transcriptomic loads (*TSHR*, *IL6*, *IL6R*) and orthogonal gene module decomposition of transcriptional pathways governing tocilizumab response (Fig. S6; see Methods, Gene-level pathway decomposition). Longitudinal transcriptomic profiling revealed tightly synchronized shifts that directly parallel serum autoantibody flares, circulating inflammatory markers, and clinical disease transitions (Fig. 1). During baseline (t0-t1), peripheral transcript loads remained quiescent, with low basal expression across Clusters C1-C5, while serum thyroid hormones (free T4/T3) and inflammatory markers (CRP, IL-6) remained strictly within normal reference ranges. Acute GD disease onset (t2) coincides with a transient surge in peripheral *TSHR* expression and circulating *IL6*, directly mirroring spikes in serum TSI, anti-TPO, and IL-6 protein. Pathway decomposition reveals selective, high-level activation of C5, signaling a massive systemic innate inflammatory wave characterized by marked myeloid

activation (*CD14, SOCS3, FCGR3A*) and chemokine release (*CXCL1, CXCL11*) during early hyperthyroid presentation. Transcriptomically, this treatment phase quieted the IL-6/JAK/STAT3 axis through a step-wise silencing of the C5 acute myeloid cascade, driving overall transcript loads to a longitudinal nadir at t5 as systemic myeloid activation is quieted, alongside a temporary peak in interferon-responsive transition elements (*CXCL9*, *IL2RA*). The emergence of TED (t6), coincided transcriptomically with a sharp, isolated global peak in peripheral *TSHR* expression and an *IL6R* rebound, directly matching retrobulbar discomfort, proptosis, and diplopia onset despite stable serum thyroid hormone levels. Here, pathway decomposition marked a distinct functional pivot away from primary myeloid inflammation toward synchronized activation of C1/2/4 and C3. This transition could reflect adaptive lymphocyte recruitment, orbital tissue homing, and active lymphocyte-fibroblast cross-talk heavily driven by IL-6 and T/B-cell cytokine receptor signaling (*IL4R*, *IL7*, *IL2RG*, *IL6*). Following steroid pulse therapy (t7), which induced rapid, transient immunosuppression by sharply dropping peripheral transcript loads and repressing both myeloid (C5) and lymphoid signaling modules (C1/2/4). During IL-6R blockade and target engagement (t8-t9), triggered a dramatic molecular shift by milestone t9. While serum CRP normalized and serum IL-6 protein exhibited classic antibody-bound dynamic changes, peripheral transcript loads of *IL6R* and *IL6* surged to global peaks. Pathway decomposition at t9 revealed profound, dense transcriptional accumulation across both myeloid (C5) and lymphoid cytokine receptor modules (C1/2/4). Rather than signaling functional downstream pathway activation, this massive single-timepoint jump represents a classic biological signature of target engagement and receptor blockade. Tocilizumab binds membrane-bound and soluble IL-6R, blocking downstream IL-6 trans-signaling and preventing receptor internalization. In response to functional blockade, immune cells upregulate transcriptional feedback loops (*IL6R*, *STAT3*, *SOCS1*, *JAK2*) in an attempt to restore homeostatic signaling capacity [Kang, 2019]. This creates a striking divergence where high transcript expression of regulatory pathway elements reflects compensatory accumulation, while downstream operational proteins and inflammatory output are functionally neutralized by the drug. Altogether, these dynamic transitions indicate that the expansion and persistent activation of pathogenic T-cell clones drive the long-lasting phase of GD with active GO/TED via sustained upregulation of the inflammatory response.

Discussion

Longitudinal immune tracking represents a paradigm shift in precision immunology, transitioning management from reactive, symptom-driven interventions to real-time, molecular monitoring. Standard diagnostics rely primarily on static blood panels; however, circulating serum biomarkers frequently uncouple from active pathology during localized tissue inflammation and targeted immunomodulation. Here, we present a compelling proof-of-concept for dynamic, intra-individual tracking in a patient with Graves' disease (GD) and corticosteroid-refractory Graves' orbitopathy (GO/TED). Serial monitoring across her clinical trajectory, from pre-symptomatic baseline to biologic-induced remission, demonstrated that the osLifetime platform, combining Immune Age

and Inflammaging/Senescence scoring, provided an accurate readout of ongoing immunopathology (autoimmune thyroid disease) where routine serology was not able to capture subtle variations.

The patient's risk profile was highly instructive. Classical hereditary susceptibility was absent; as she lacked canonical GD risk haplotype (HLA class II: DRB1*03 (DR3), DQA1*05:01, and DQB1*02:01) standard for European cohorts [Khong 2016; Limbach 2016]. Instead, environmental and endocrine triggers (active smoking and the postpartum state) coincided with a maternal history of autoimmunity and thyroid disorders to drive the disease onset. Crucially, even within well-studied populations, static genomics can fail to capture non-classical polygenic variants or complex environmental interactions. This limitation highlights where dynamic tracking supersedes static genomics by establishing an internal reference where the patient serves as her own control.

Her clinical course also illustrated the well-known dissociation between thyroid axis status and orbital disease activity. Although antithyroid therapy normalized thyroid hormones, TSI remained elevated and orbitopathy flared [Hoang 2022; Lanzolla 2024; Pérez-Moreiras 2021]. Relying on thyroid hormones alone would have masked active tissue-level disease, a failure mode directly resolved by osLifetime immune-level tracking.

Therapeutically, the trajectory followed an evidence-based escalation pathway. First-line high-dose methylprednisolone failed due to non-response and rising intraocular pressure, a refractory course likely exacerbated by active smoking, the single strongest modifiable risk factor for orbitopathy and corticosteroid resistance [Bartalena 2021; Su 2026]. Second-line IL-6 receptor blockade with tocilizumab was initiated per EUGOGO guidelines for steroid-refractory, moderate-to-severe active orbitopathy, reflects the central role of IL-6 in orbital fibroblast activation and CD4+ T-cell differentiation [Fang 2021; Zhou 2026; Chen 2021]. Rapid orbital recovery occurred despite persistently positive TSI, mirroring trial data where anti-IL-6R therapy improved proptosis and activity scores independent of TSI clearance [Pérez-Moreiras 2018, 2021]. Mechanistically, the post-initiation surge in total serum IL-6 reflects receptor saturation and inhibited receptor-mediated clearance, confirming target engagement.

Beyond informing GO/TED management, this case demonstrates the capacity of longitudinal osLifetime profiling to dissect distinct immune modalities: Inflammaging and Senescence, which act as coupled, as high-velocity indicators of acute effector signaling (immune "weather"), and Immune Age, which tracks slower, structural cellular pool remodeling and systemic capacity (immune "climate"). This dual framework was evident across the disease course. In the acute flare phase, a transient drop in Immune Age (to 26.7 years; chronological age 39.1, Δ = -12.4) indexed effector-skewed T-cell mobilization under autoimmune drive. Under corticosteroid pulse therapy, moderate negative Inflammaging and Senescence *z*-scores registered systemic suppression while capturing the lack of localized orbital response. Upon IL-6R blockade, osLifetime tracked genuine tissue resolution and rapid clinical recovery as its Inflammaging Score plummeted to 0.707 (z = -2.509) (mirrored by a suppressed Senescence Score of 0.777 (z = -1.097)) in step with visual recovery, despite the expected serum IL-6 surge. Finally, amid treatment withdrawal, the parallel rise of the Inflammaging (0.835; z = +1.739) and Senescence

(0.851; z = +0.644) scores acted as an early-warning radar to detect subclinical reactivation ahead of clinical symptoms. The synchronized trajectory of these scores across both treatment and withdrawal underscores their linked biology, demonstrating that while resolving systemic inflammation cools the cellular stress pathways driving immune exhaustion, the re-emergence of senescent cells actively fuels recurrent inflammation through their secretory phenotype [Yin 2025].

Throughout the disease continuum, Immune Age demonstrated greater utility for longitudinal monitoring compared to standard TCR repertoire metrics. While basic feature-level indices such as richness and clonality fluctuated sharply during early disease phases (t2-t3) and ATD tapering (t4-t5), Immune Age exhibited a continuous, steady decline. This trajectory reliably captured the intense cellular mobilization driving the immunopathology and through the course of treatment. While feature-level deconstruction of TCR dynamics resolves specific clonal shifts, it is the integration of these features into system-level metrics like Immune Age that successfully captures linear disease progression. Mechanistically, this phenomenon arises because the intense mobilization and peripheral restructuring of T-cell subsets alter the transcriptomic and TCR profiles toward features characteristic of younger immune systems. Consequently, a decreasing Immune Age should not be misconstrued as immunological rejuvenation, but rather recognized as a quantitative readout of active, subclinical cellular turnover and tissue homing during autoimmune progression.

Where system-level scores such as Immune Age capture the disease trajectory, targeted molecular deconstruction tries to resolve its underlying drivers. By combining event-related TCR analysis with transcriptional profiling, this approach allowed us to pinpoint the specific clonal and inflammatory programs propelling the disease course and mediating the response to therapy. While these granular molecular findings remain hypothesis-generating in this single-patient design, they demonstrate the platform's capacity to trace macro-level clinical outcomes back to their precise cellular origins.

Key strengths of this study include the availability of pre-disease baseline samples, dense serial timepoints during disease course and therapeutic intervention, and the elimination of inter-individual background variation within a single genetic background. Certain limitations remain: as a single-patient study, these findings are hypothesis-generating; the antigen specificity of expanded T-cell clones requires functional validation; and if peripheral blood serves as a proxy for the retrobulbar (intrathyroidal and orbital) tissue compartments [Wang 2020; Fang 2021]. Additionally, as a potential clinical confounder, supportive lifestyle measures coincided with biologic initiation. However, lifestyle changes cannot induce receptor-saturation kinetics or systemic IL-6 accumulation. The synchronized collapse of the Inflammaging Score alongside this target-engagement biomarker confirms that recovery was fundamentally driven by IL-6R blockade.

Current GD-GO/TED management remains predominantly reactive, relying on overt symptoms and late systemic markers. Longitudinal profiling through the osLifetime platform offers a biology-level roadmap: tracking the immune response, anticipated subclinical flares and differentiated ineffective treatments from targeted successes in real time. The logical extension of this

paradigm is tracking autoreactive T-cell populations in real time, bridging early clonal detection to emerging immunotherapies such as TSHR-directed CAAR T cells and peptide vaccines [Cheever 2025; Lanzolla 2024].

Conclusion

This case provides a clear proof-of-concept for longitudinal immune tracking through the osLifetime platform in complex autoimmunity. By capturing a true pre-symptomatic baseline, the platform enabled precise benchmarking of disease progression across therapeutic transitions. Furthermore, longitudinal monitoring revealed subclinical flares, exposed the blind spots of standard serology, and registered tissue-level remission in real time.

Clinical Insights

PATIENT PERSPECTIVE

"For nearly a year, I was misdiagnosed with conjunctivitis by three separate ophthalmologists. I was given corticosteroid treatments that didn't work while my vision progressively worsened, causing double vision and visible changes to my eyes that deeply affected my self-image. It was frustrating and distressing to live with such unpredictability and feel so helpless without clear answers. The turning point came when I took a medical leave to eliminate screen time and focus entirely on my health. I switched to targeted antibody therapy, started red-light heat therapy to restore my natural tear production, and adopted an anti-inflammatory diet alongside regular exercise and proper sleep. Within days, my sight improved for the first time in months. Being able to track my own immune data across that entire period replaced the guesswork with clarity."
- ***The patient***

CLINICIAN PERSPECTIVE

"The management of GO/TED is often clinically challenging. In this case, the first challenge was that the systemic symptoms of thyrotoxicosis coincided with the postpartum and lactation period delaying diagnosis and management. The second challenge was the dissociation between standard serum biochemistry, subclinical symptoms and active immunopathology at the molecular level. This is evidenced by the improvement in thyroid function and thyroid autoimmune serology and normal serum inflammatory markers while on treatment with thiamazole while the patient went on to develop severe corticosteroid resistant GO/TED requiring a shift from broad immunosuppression to targeted biologic therapy. Subsequently, during administration of the first tocilizumab protocol, standard serology markers (except for artificial surge in IL-6) remained stable so gauging response to treatment at the molecular level was compromised. Furthermore, anticipating symptom recurrence following protocol completion proved challenging when relying solely on standard serological markers.

What makes this case unique and instructive was having parallel access to deep longitudinal immune profiling through the osLifetime platform which served as an indispensable biological compass. Standard serology markers' normal value ranges are based on population averages and so are not the best tools to capture early shifts in the immune system function in autoimmune conditions. Nonetheless, in practice, these are the main tools available to clinicians to manage and monitor complex autoimmune disease progression. In this case, osLifetime established an intra-individual reference frame prior to symptom onset and through deep longitudinal tracking, signalled acute inflammatory surges at the cellular level forecasting reactivation before peak clinical symptoms re-emerged allowing for timely therapeutic re-engagement. Furthermore, real-time tracking revealed an improvement in Inflammaging score on initiating tocilizumab, mirroring intracellular signaling suppression and visual recovery.

This case demonstrates that osLifetime is an important tool for healthcare professionals managing complex autoimmune disease. This approach moves us past the blind spots of static population-averaged snapshots, toward continuous personalized immune profiling providing clinicians with a precise and actionable roadmap to successfully navigate treatment resistance, achieve remission and ultimately improve the quality of life of the patient."
*- **Dr. Roberta Vella Azzopardi, PhD** (Medical Doctor Specialist in Longevity Medicine, Clinical Nutrition, and Women's Health; Elyside Concierge Clinic, Saint James Hospital Group. Clinical Advisor, Omniscope)*

Supplementary Figures

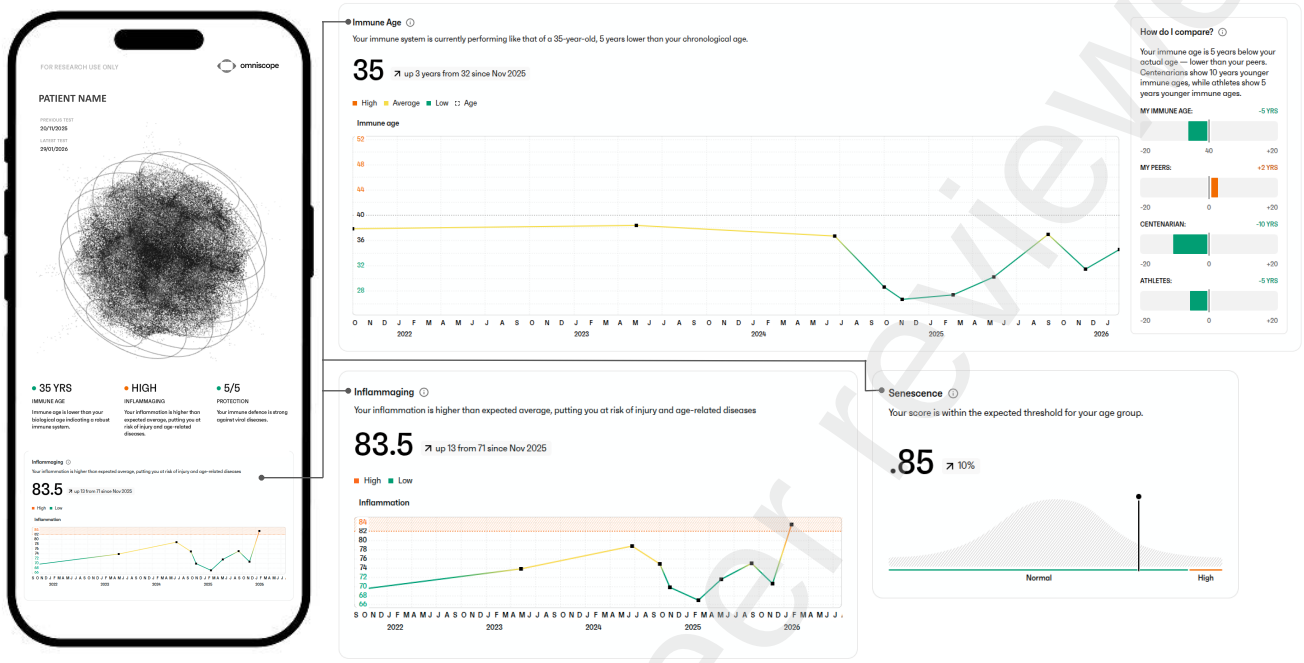

Figure S1. Mobile app dashboard for real-time patient monitoring and disease trajectory tracking via osLifetime. (**Left**) Mobile interface displaying the patient's multidimensional immune representation (Cellular Avatar) alongside summary metrics for Immune Age and Inflammaging. (**Right**) Expanded graphical readouts displaying the longitudinal tracking of the patient's predicted Immune Age, including benchmark comparisons to peers, centenarians, and athletes on said time point (**top**); Inflammaging Score spanning pre-onset to post-remission (**bottom-left**); and, a snapshot of the Senescence Score at t9 (**bottom-right**). *Note: These interface views were downloaded following timepoint t9.*

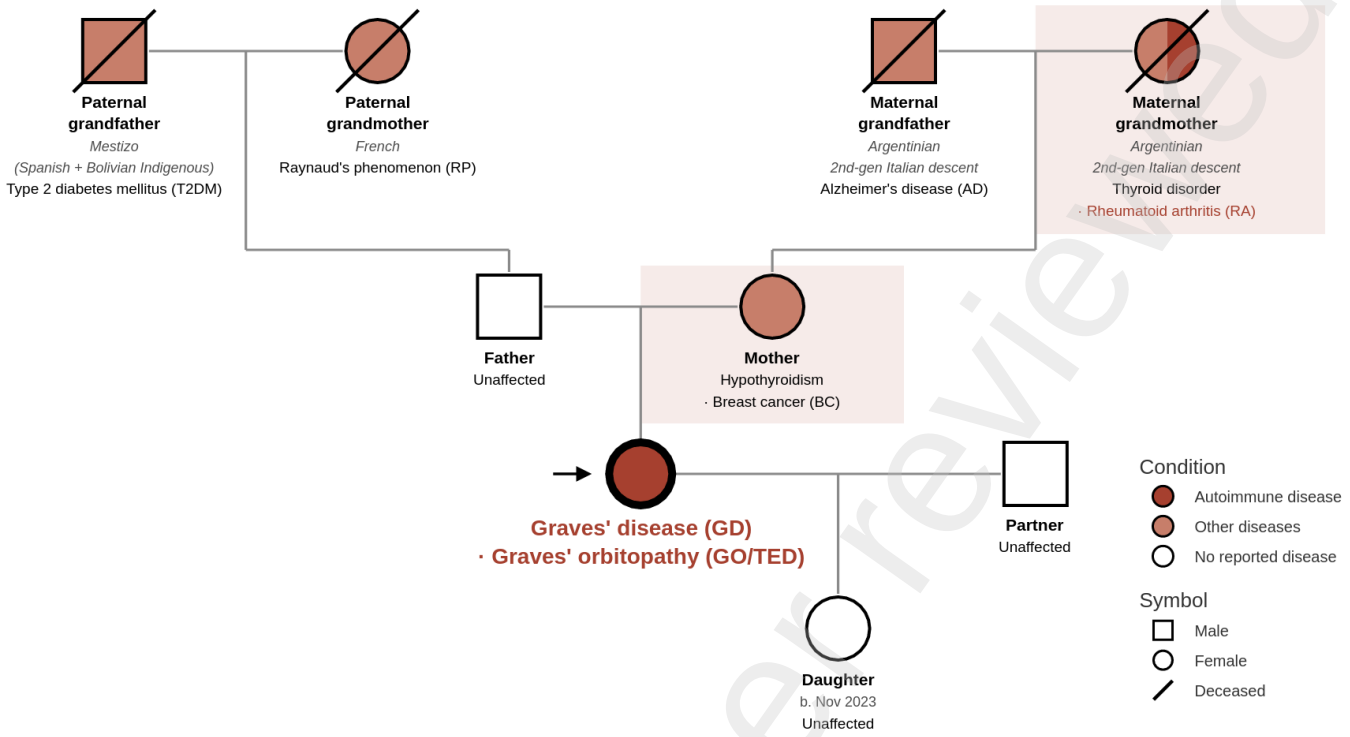

Figure S2. Family pedigree illustrating maternal-line clustering of autoimmune and systemic diseases. The patient (black arrow) presented with Graves' Disease (GD) and Graves' Orbitopathy / Thyroid Eye Disease (GO/TED). Maternal lineage demonstrates an aggregation of autoimmune and thyroid disorders, including a grandmother with an undiagnosed thyroid disease and Rheumatoid Arthritis (RA), and a grandfather with Alzheimer's disease (AD). The patient's mother had Hypothyroidism (since menarche) and Breast Cancer (BC). The paternal lineage shows a grandmother with Raynaud's Phenomenon (RP), a grandfather with Diabetes Mellitus (DM), and an unaffected father. The patient's partner and daughter (born November 2023) are currently unaffected. *Symbols:* Squares represent males; circles represent females. Dark red shading indicates autoimmune conditions; light brownish shading indicates other non-autoimmune conditions; white shapes indicate unaffected individuals or no reported disease.

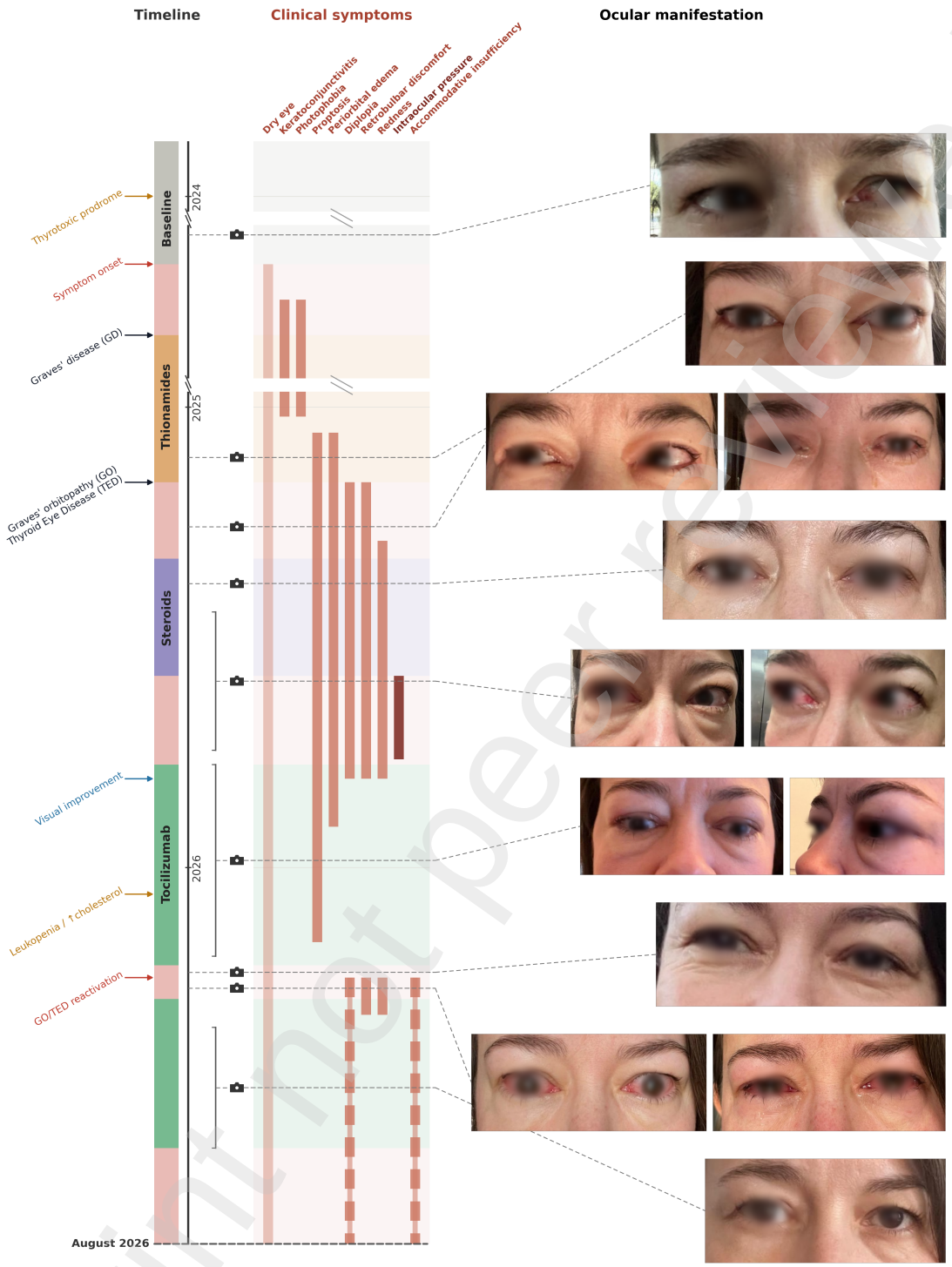

Figure S3. Clinical observation window and longitudinal photographic evolution of ocular manifestations and Graves' orbitopathy (GO/TED). Serial clinical photography illustrates the patient's ocular disease trajectory across key clinical timepoints; Double slash marks indicating timeline breaks between evaluations. Initial presentation shows isolated superior limbic keratoconjunctivitis (SLK) and ocular surface breakdown, preceding the onset of active moderate-to-severe GO marked by significant acute orbital inflammation and extraocular muscle dysfunction. Intravenous corticosteroid pulse therapy produces transient anti-inflammatory relief, followed by steroid-resistant rebound, clinical deterioration, and systemic cushingoid side effects leading to drug cessation. Transition to targeted IL-6 receptor blockade via tocilizumab induces rapid suppression of active orbital tissue inflammation, reduction of proptosis, and restoration of extraocular motility. Temporary drug withdrawal triggers minor localized inflammatory reactivation, which resolves completely following re-treatment, demonstrating sustained disease quiescence and complete inactivation of GO/TED. The irises have been digitally blurred in all panels to reduce identifiability.

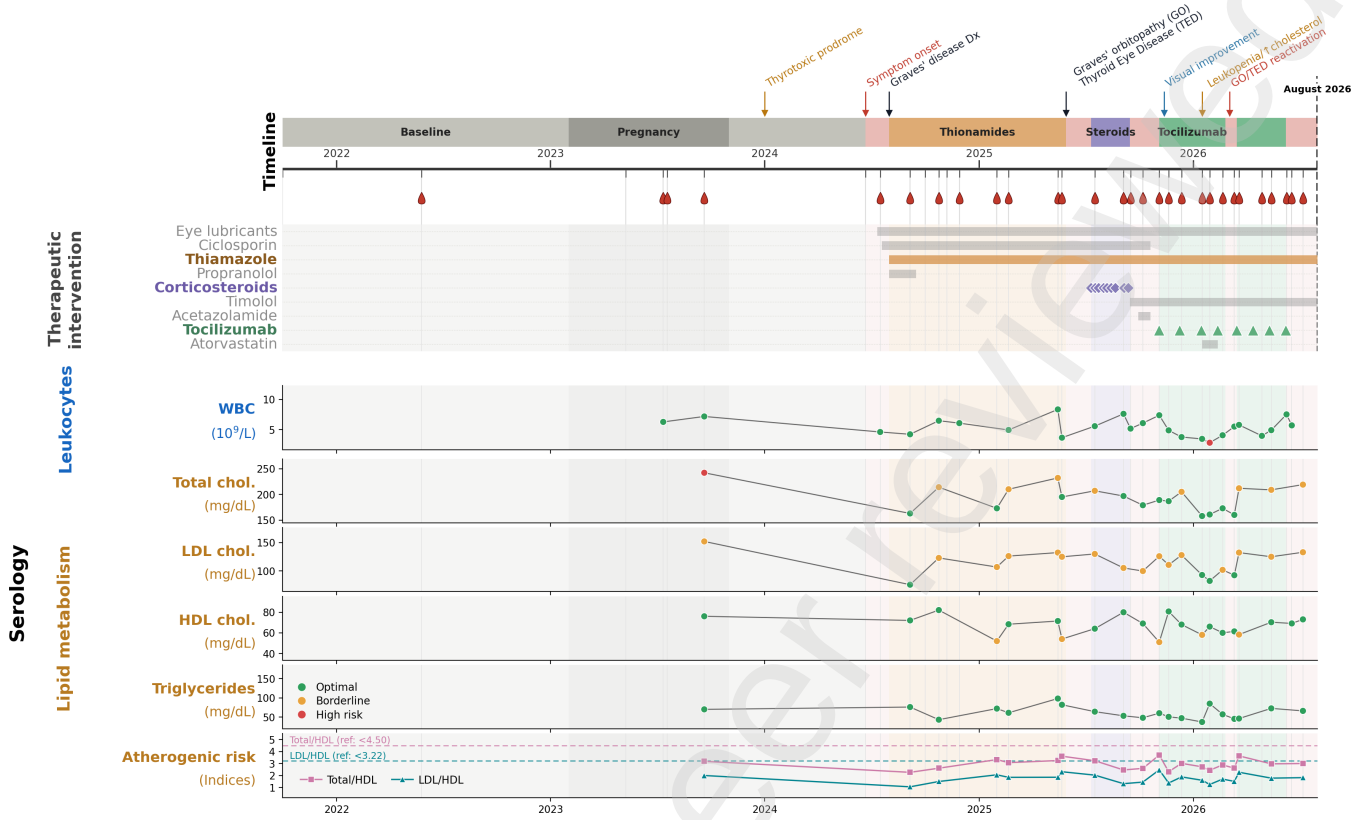

Figure S4. Longitudinal blood panel dynamics across clinical disease phases and therapeutic interventions, with a focus on tocilizumab therapy. (Top) Timeline of clinical events, blood sampling sources, and therapeutic administration, including thionamides, corticosteroids, and tocilizumab. Blood icons indicate routine clinical laboratory panels. **(Bottom)** Routine serology panels. Leukocytes: Serial white blood cell (WBC) count. Lipid Metabolism: Longitudinal tracking of Total Cholesterol, LDL cholesterol, HDL cholesterol, Triglycerides, and Atherogenic Risk ratios (Total:HDL and LDL:HDL). Individual data points across panels are color-coded by clinical reference bands: green indicates optimal/normal values, orange indicates borderline values, and red indicates high-risk values outside reference limits. Dashed horizontal lines indicate female reference population optimal thresholds for risk ratios.

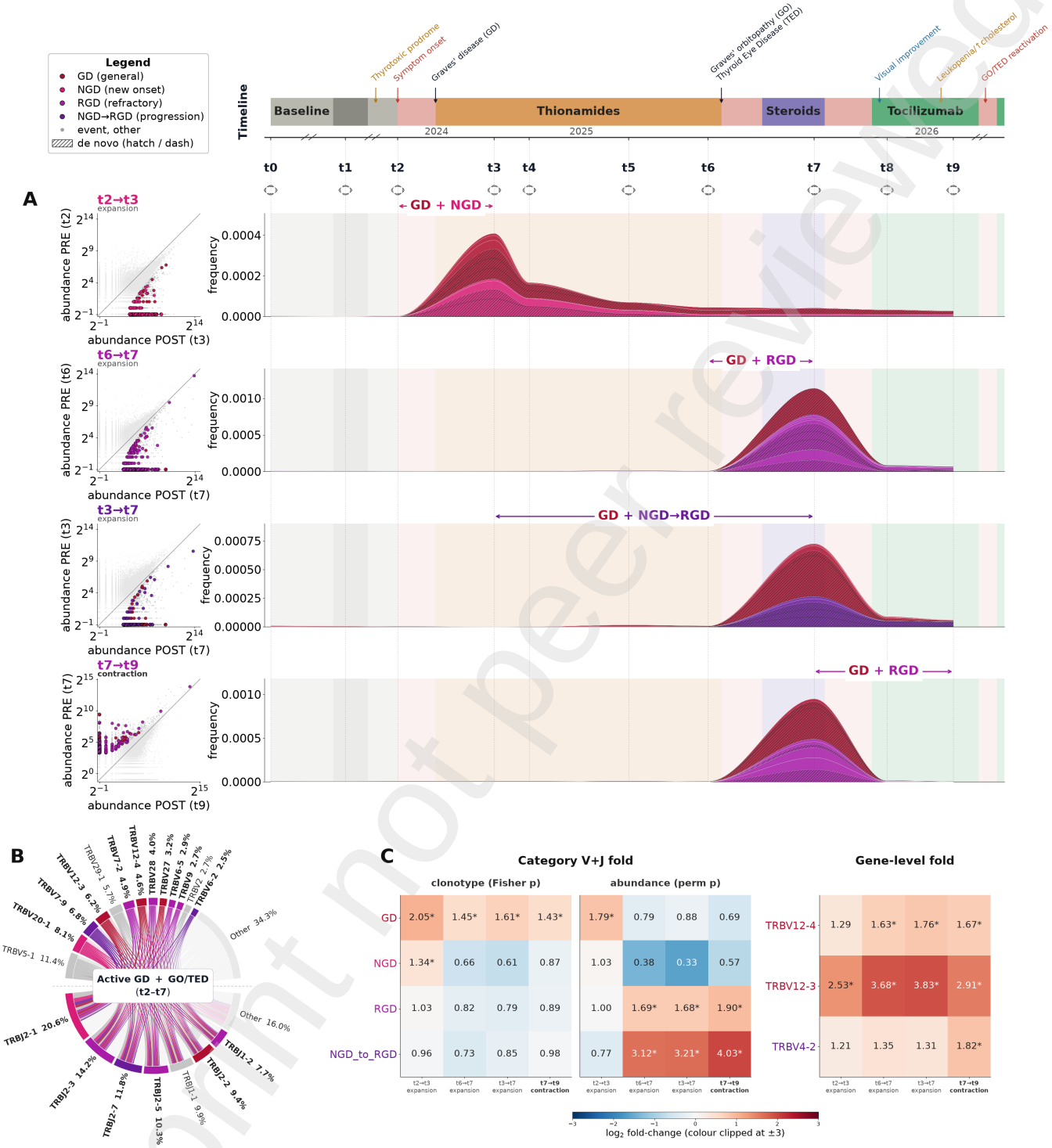

Figure S5. Deep T-cell receptor (TCR)-sequencing repertoire dynamics across the disease course. (A) For each interval, the scatter shows the PRE versus POST abundance of every event-related clonotype (log2 axes; zero-abundance floored). Concrete disease-associated V∧J clonotypes are highlighted over the grey background of all other event clones. The adjacent stacked-area panel tracks, over all ten samples (t0-t9), the frequency of the ten disease-associated clonotypes with the largest fold-change in that interval's event direction, restricted to five de novo (hatched) and five pre-existing (solid) clones. Each interval is labelled with the direction of its event test (expansion, or contraction for the therapy interval) and with the disease-stage hypothesis it evaluates. Abbreviations of disease stage refer to: GD, General Graves' disease; NGD, Newly diagnosed disease; RGD, Refractory disease; NGD-RGD, Progression drivers. Timepoints are vertically aligned to the clinical timeline. **(B)**

Circos-style chord diagram of TRBV-TRBJ pairing over the pooled active-disease window (t2-t7): the upper semicircle carries TRBV, the lower TRBJ, and each ribbon's width is proportional to that pair's share of the pooled repertoire. Arc and ribbon colour encode the literature disease class. **(C)** Clonotype-level (Fisher) and abundance-level (permutation) enrichment fold-changes of the disease-associated V∧J compartment, shown per stage class (GD / NGD / RGD / NGD-RGD) and per individual TRBV/TRBJ segment. Only segments reaching the enrichment threshold (fold ≥ 1.5) in at least one interval are displayed, and cells are marked with an asterisk at fold ≥ 1.5 and p < 0.05. Colour encodes log2 fold-change (clipped at ±3).

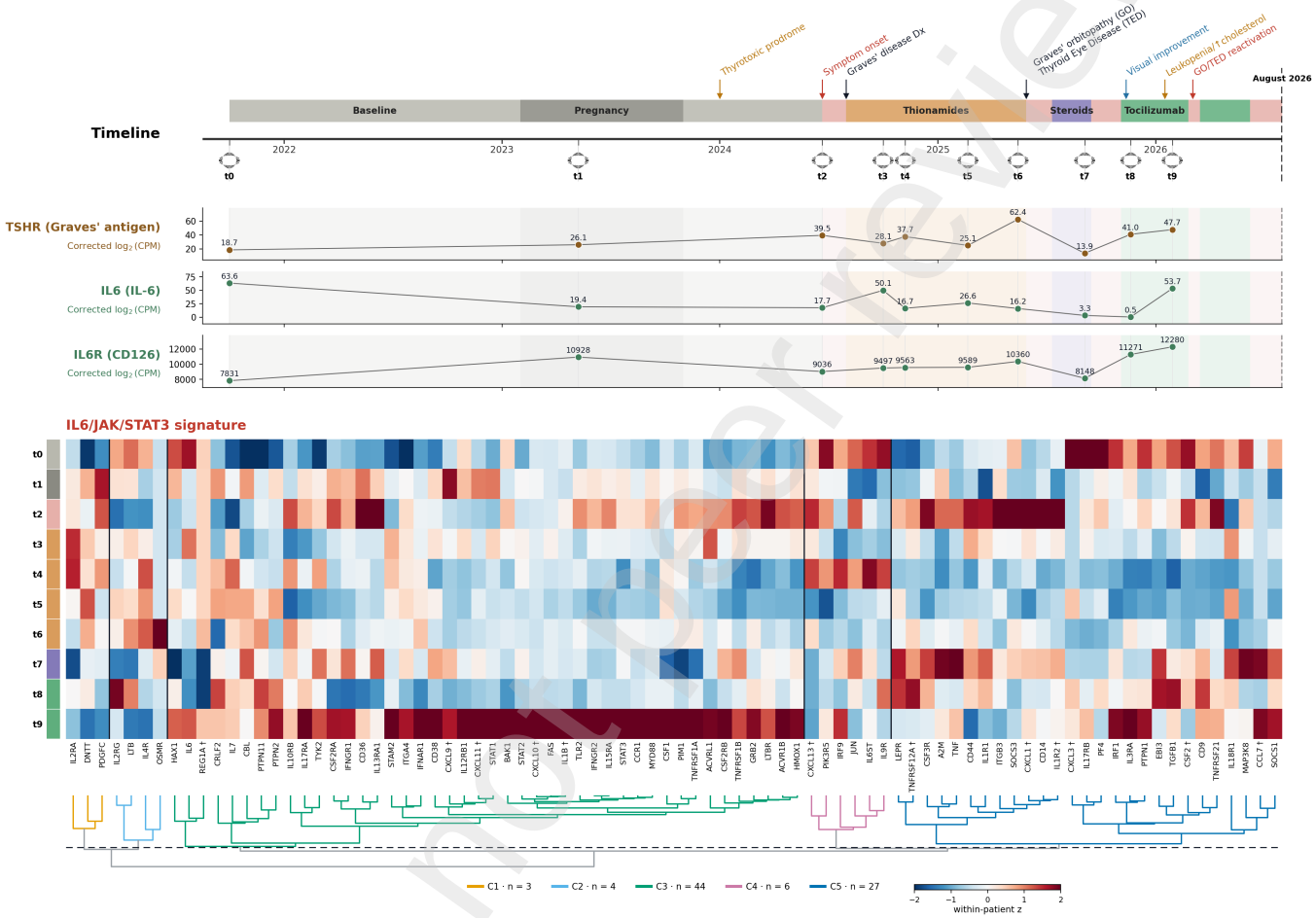

Figure S6. Longitudinal clinical timeline, therapeutic regimens, and transcriptomics dynamics. (**Top**) Overview of key disease milestones mapped alongside therapeutic phases and osLifetime sampling intervals (t0-t9). (**Middle**) *TSHR*, *IL6* and *IL6R* gene expression. Values represent anchored corrected CPM. (**Bottom**) Decomposed "HALLMARK_IL6_JAK_STAT3_SIGNALING" gene programme (84/87 genes). Values displayed as within-patient z clipped to ±2. Genes were clustered by average linkage on correlation distance and cut into five clusters (dendrogram below, coloured by cluster, links above the cut in grey). The dagger (†) marks genes with sub-floor corrected CPM at one or more draws (12 of 84).

References

Antonelli, A., Fallahi, P., Elia, G., Ragusa, F., Paparo, S. R., Ruffilli, I., Patrizio, A., Gonnella, D., Giusti, C., Virili, C., Centanni, M., Shoenfeld, Y., & Ferrari, S. M. (2020). Graves' disease: Clinical manifestations, immune pathogenesis (cytokines and chemokines) and therapy. *Best Practice & Research Clinical Endocrinology & Metabolism*, 34(1), 101388. https://doi.org/10.1016/j.beem.2020.101388

Bartalena, L., Kahaly, G. J., Baldeschi, L., Dayan, C. M., Eckstein, A., Marcocci, C., Marinò, M., Vaidya, B., Wiersinga, W. M., & the European Group on Graves' Orbitopathy (EUGOGO). (2021). The 2021 European Group on Graves' Orbitopathy (EUGOGO) clinical practice guidelines for the medical management of Graves' orbitopathy. *European Journal of Endocrinology*, 185(4), G43-G67. https://doi.org/10.1530/EJE-21-0479

Burch, H. B., Perros, P., Bednarczuk, T., Cooper, D. S., Dolman, P. J., Leung, A. M., Mombaerts, I., Salvi, M., & Stan, M. N. (2022). Management of thyroid eye disease: A consensus statement by the American Thyroid Association and the European Thyroid Association. *Thyroid*, 32(12), 1439-1470. https://doi.org/10.1089/thy.2022.0251

Cheever, A., Lindsay, H. G., Kang, C. C., Hansen, M., Demars, K., O'Neill, K. L., & Weber, K. S. (2025). Chimeric autoantibody receptor T cells specifically eliminate Graves' Disease autoreactive B cells. *Frontiers in Immunology*, *16*. https://doi.org/10.3389/fimmu.2025.1562662

Chen, Z., Liu, Y., Hu, S., Zhang, M., Shi, B., & Wang, Y. (2021). Decreased Treg cell and TCR expansion are involved in long-lasting Graves' disease. *Frontiers in Endocrinology*, 12, 632492. https://doi.org/10.3389/fendo.2021.632492

Fang, S., Lu, Y., Huang, Y., Zhou, H., & Fan, X. (2021). Mechanisms that underly T cell immunity in Graves' orbitopathy. *Frontiers in Endocrinology*, 12, 648732. https://doi.org/10.3389/fendo.2021.648732

Hoang, T. D., Stocker, D. J., Chou, E. L., & Burch, H. B. (2022). 2022 update on clinical management of Graves' disease and thyroid eye disease. *Endocrinology and Metabolism Clinics of North America*, 51(2), 287-304. https://doi.org/10.1016/j.ecl.2021.12.004

Jia, X., Zhai, T.-Y., Wang, B., Zhang, J.-A., & Song, R.-H. (2022). High-throughput T cell receptor sequencing reveals differential immune repertoires in autoimmune thyroid diseases. *Molecular and Cellular Endocrinology*, 550, 111644. https://doi.org/10.1016/j.mce.2022.111644

Kang, S., Tanaka, T., Narazaki, M., & Kishimoto, T. (2019). Targeting Interleukin-6 Signaling in Clinic. Immunity, 50(4), 1007–1023. https://doi.org/10.1016/j.immuni.2019.03.026

Ke, S., Liu, Z., Zhou, M., Xiao, B., Hu, Q., Lin, J., Ye, H., Luo, L., & Lin, X. (2025). Single-cell multiomic analysis unveils the immune landscape dynamics of Graves' ophthalmopathy. *Communications Biology*, 8, 732. https://doi.org/10.1038/s42003-025-08115-7

Khong, J. J., Burdon, K. P., Lu, Y., Laurie, K., Leonardos, L., Baird, P. N., Sahebjada, S., Walsh, J. P., Gajdatsy, A., Ebeling, P. R., Hamblin, P. S., Wong, R., Forehan, S. P., Fourlanos, S., Roberts, A. P., Doogue, M., Selva, D., Montgomery, G. W., Macgregor, S., & Craig, J. E. (2016). Pooled genome wide association detects association upstream of FCRL3 with Graves' disease. *BMC Genomics*, 17, 939. https://doi.org/10.1186/s12864-016-3276-z

Kim, D. W., Kim, S., Han, J., Belday, K., Li, E., Mahoney, N., Blackshaw, S., & Rajaii, F. (2024). Transcriptomic profiling of thyroid eye disease orbital fat demonstrates differences in adipogenicity and IGF-1R pathway. *JCI Insight*, 9(24), e182352. https://doi.org/10.1172/jci.insight.182352

Lanzolla, G., Marinò, M., & Menconi, F. (2024). Graves disease: Latest understanding of pathogenesis and treatment options. *Nature Reviews Endocrinology*, 20(11), 647-660. https://doi.org/10.1038/s41574-024-01016-5

Limbach, M., Saare, M., Tserel, L., Kisand, K., Eglit, T., Sauer, S., Axelsson, T., Syvänen, A.-C., Metspalu, A., Milani, L., & Peterson, P. (2016). Epigenetic profiling in CD4+ and CD8+ T cells from Graves' disease patients reveals changes in genes associated with T cell receptor signaling. *Journal of Autoimmunity*, 67, 46-56. https://doi.org/10.1016/j.jaut.2015.09.006

Liu, Z., Ke, S.-R., Shi, Z.-X., Zhou, M., Sun, L., Sun, Q.-H., Xiao, B., Wang, D.-L., Huang, Y.-J., Lin, J.-S., Wang, H.-S., Zhang, Q.-K., Pan, C.-N., Liang, X.-W., Chen, R.-X., Mao, Z., & Lin, X.-C. (2024). Dynamic transition of Tregs to cytotoxic phenotype amid systemic inflammation in Graves' ophthalmopathy. *JCI Insight*, 9(22), e181488. https://doi.org/10.1172/jci.insight.181488

Maliah, A., Parikh, R., Tayer-Shifman, O. E., Kimhi, O., Gepstein, R., Halperin, T., Levy, Y., Levy, C., Pri-Paz Basson, Y., & Kivity, S. (2022). Steroid treatment suppresses the CD4+ T-cell response to the third dose of mRNA COVID-19 vaccine in systemic autoimmune rheumatic disease patients. Scientific reports, 12(1), 21056. https://doi.org/10.1038/s41598-022-25642-z

Nada, A. M., & Hammouda, M. (2014). Immunoregulatory T cells, LFA-3 and HLA-DR in autoimmune thyroid diseases. *Indian Journal of Endocrinology and Metabolism*, *18*(4), 574-581. https://doi.org/10.4103/2230-8210.137524

Pérez-Moreiras, J. V., Gómez-Reino, J. J., Maneiro, J. R., Pérez-Pampín, E., Romo López, A., Rodríguez Álvarez, F. M., Castillo Laguarta, J. M., Del Estad Cabello, A., Gessa Sorroche, M., España Gregori, E., & Sales-Sanz, M. (2018). Efficacy of tocilizumab in patients with moderate-to-severe corticosteroid-resistant Graves orbitopathy: A randomized clinical trial. *American Journal of Ophthalmology*, 195, 181-190. https://doi.org/10.1016/j.ajo.2018.07.038

Pérez-Moreiras, J. V., Varela-Agra, M., Prada-Sánchez, M. C., & Prada-Ramallal, G. (2021). Steroid-resistant Graves' orbitopathy treated with tocilizumab in real-world clinical practice: A 9-year single-center experience. *Journal of Clinical Medicine*, 10(4), 706. https://doi.org/10.3390/jcm10040706

Qi, Q., Liu, Y., Cheng, Y., Glanville, J., Zhang, D., Lee, J. Y., Olshen, R. A., Weyand, C. M., Boyd, S. D., & Goronzy, J. J. (2014). Diversity and clonal selection in the human T-cell repertoire. Proceedings of the National Academy of Sciences of the United States of America, 111(36), 13139-13144. https://doi.org/10.1073/pnas.1409155111

Ross, D. S., Burch, H. B., Cooper, D. S., Greenlee, M. C., Laurberg, P., Maia, A. L., Rivkees, S. A., Samuels, M., Sosa, J. A., Stan, M. N., & Walter, M. A. (2016). 2016 American Thyroid Association guidelines for diagnosis and management of hyperthyroidism and other causes of thyrotoxicosis. *Thyroid*, 26(10), 1343-1421. https://doi.org/10.1089/thy.2016.0229

Su, Y., & Cao, J. (2026). Smoking-induced HLA-DQA1 overexpression in T cells: A novel pathway in thyroid eye disease development. *Frontiers in Immunology*, 17, 1745010. https://doi.org/10.3389/fimmu.2026.1745010

Tanaka, T., Narazaki, M., & Kishimoto, T. (2011). Anti-interleukin-6 receptor antibody, tocilizumab, for the treatment of autoimmune diseases. FEBS letters, 585(23), 3699-3709. https://doi.org/10.1016/j.febslet.2011.03.023

Volpé R. (2001). The immunomodulatory effects of anti-thyroid drugs are mediated via actions on thyroid cells, affecting thyrocyte-immunocyte signalling: a review. Current pharmaceutical design, 7(6), 451-460. https://doi.org/10.2174/1381612013397898

Wang, Y., Liu, Y., Yang, X., Guo, H., Lin, J., Yang, J., He, M., Wang, J., Liu, X., Shi, T., Wu, L., Zhang, C., Ye, K., & Shi, B. (2020). Predicting the early risk of ophthalmopathy in Graves' disease patients using TCR repertoire. *Clinical and Translational Medicine*, 10(7), e218. https://doi.org/10.1002/ctm2.218

Wang, Y., Chen, Z., Wang, T., Guo, H., Liu, Y., Dang, N., Hu, S., Wu, L., Zhang, C., Ye, K., & Shi, B. (2021). A novel CD4+ CTL subtype characterized by chemotaxis and inflammation is involved in the pathogenesis of Graves' orbitopathy. *Cellular & Molecular Immunology*, 18(3), 735-745. https://doi.org/10.1038/s41423-020-00615-2

Yang, H., Bi, X., Tang, H., Zeng, J., Cong, Y., Wu, T., & Chen, Q. (2015). Clinical efficacy of Yingliu treatment for Graves disease. International journal of clinical and experimental medicine, 8(4), 6145-6153. PMID: 26131218

Yin, F., He, Y., Li, J., & Gao, Y. (2025). Immune cell senescence in autoimmunity: implications for disease pathogenesis and therapeutic targeting. Frontiers in immunology, 16, 1596686. https://doi.org/10.3389/fimmu.2025.1596686

Zhou, X., Cong, J., Peng, R., Yang, D., Dong, C., Xie, J., Yan, J., Kuang, J., Li, F., Yeap, L. S., Xie, X., Yin, H., Han, R., Shen, L., Zhou, Y., Ning, G., Wang, S., Wang, W., & Ye, L. (2026). Single-cell RNA sequencing of thyroid tissues reveals pathogenesis of Graves' disease. *Advanced Science*, 13(1), e08449. https://doi.org/10.1002/advs.202508449

Materials and Methods

This study combines standard-of-care clinical laboratory monitoring with non-routine molecular and computational immune-profiling assays performed within the osLifetime platform. The derived metrics and their interpretation are defined below.

Study design. This was a single-participant (n = 1), longitudinal study in which the participant serves as her own within-subject control.

Clinical laboratory assay. Routine clinical and endocrine monitoring was performed throughout the disease course at accredited clinical laboratories (Cerba, Sanitas, Centro de Análisis Sanitarios (CAS), Eurofins), each using its own standard assays and reference ranges. Laboratory measurements were programmatically extracted from the source clinical reports, harmonised to conventional units, and annotated with a single reference interval per analyte (taken from the primary laboratory); where reference ranges differed between laboratories or over time, each measurement retain each laboratory's own assay cutoff and is indicated. Serial panels covered several analyte groups: (i) Thyroid function and autoantibodies, including thyroid-stimulating hormone (TSH), free triiodothyronine (free T3) and free thyroxine (free T4), thyroid-stimulating immunoglobulin (TSI/TRAb), and anti-thyroid-peroxidase (anti-TPO); (ii) Inflammatory & Cytokine markers, including serum interleukin-6 (IL-6), tumour-necrosis-factor-α (TNF-α) and C-reactive protein (CRP); and (iii) Safety & Metabolic monitoring, consisting of a complete blood counts (specifically Leukocytes) and full lipid profile (total cholesterol, high-density lipoprotein [HDL], and low-density lipoprotein [LDL]), and calculated atherogenic risk ratios (total cholesterol-to-HDL ratio [Total/HDL] and LDL-to-HDL ratio [LDL/HDL], computed directly from the individual lipid parameters). Values were interpreted relative to these reference intervals and to the participant's own pre-onset baseline, not against statistical thresholds.

osLifetime samples. Peripheral whole blood was collected at ten osLifetime timepoints (t0-t9) spanning approximately 5 year-period (2021-2026), combining routinely scheduled draws with event-driven sampling timed to clinical inflection points (symptom onset, diagnosis, and each treatment switch) (Table 1). Two samples predated clinical onset, a healthy pre-pregnancy baseline (t0) and a sample obtained during pregnancy (t1), and served as pre-disease molecular reference states. Peripheral blood mononuclear cells (PBMCs) were isolated directly from fresh blood and cryopreserved in a freezing medium. The cryopreserved PBMCs were stored at -80ºC for 24 hours before being transferred to liquid nitrogen storage.

Table 1. Longitudinal multi-omic profiling across ten osLifetime checkpoints. Summary of the patient's clinical trajectory across ten strategic timepoints (t0-t9) spanning a 5-year period (2021-2026).

OSLIFETIME TIMEPOINT	SAMPLING DATE	CLINICAL STATE
t0	**October 2021;** 2021-10-01	Baseline (Pre-symptomatic)
t1	**May 2023;** 2023-05-09	Pregnancy
t2	**June 2024;** 2024-06-21	Symptom onset
t3	**October 2024;** 2024-10-01	Acute GD
t4	**November 2024;** 2024-11-07	Acute GD Management
t5	**February 2025;** 2025-02-20	Chronic GD Management
t6	**May 2025;** 2025-05-15	GO/TED Emergence
t7	**September 2025;** 2025-09-04	Active GO/TED
t8	**November 2025;** 2025-11-20	GO/TED Improvement
t9	**January 2026;** 2026-01-29	GO/TED Remission (Pre-reactivation)

T-cell receptor (TCR) repertoire sequencing (osTCR). TCR sequencing was performed using the proprietary osTCR assay to generate sequencing-ready libraries (Omniscope, Inc., Delaware, USA). Analysis was restricted to productive TRB rearrangements and germline TRBV and TRBJ allele calls were collapsed to the gene level. A clonotype was defined by its contig identifier, comprising TRBV gene, CDR3 nucleotide sequence, and TRBJ gene. Clonotype abundance was calculated as the sum of reported counts, and frequency as the abundance divided by the sample's total counts.

osLifetime composite metrics. Different composite readouts computed by the osLifetime platform are reported: the Immune Age, and the Inflammaging and Senescence Scores. Because the Immune Age integrates remodelling of structural repertoire features, whereas the Inflammaging and Senescence scores reflect transcriptional activity, the two classes are interpreted as complementary immune readouts.

- Immune Age. Immune Age is determined using Omniscope's proprietary model (osAge) that computes an individual's predicted immunological age, expressed in years, based on sample-specific T-cell features. Results are also reported as the age deviation (Δ), calculated as predicted Immune Age minus chronological age at sampling. Generally, a positive Δ denotes accelerated immune aging, whereas a negative Δ denotes decelerated aging. However, pronounced shifts from an individual's baseline can also indicate a deep structural remodeling of the T-cell compartment. Consequently, in the context of autoimmunity, a sudden decrease in Immune Age must be interpreted strictly as an objective marker of acute immune mobilization and active clonal recruitment, rather than true biological rejuvenation.

- Inflammaging and Senescence Scores. Per-sample scores were generated using transcriptomics as input. The coordinated regulation of functionally related gene sets was quantified and summarized into a single normalized enrichment score (NES) for each sample using Omniscope's Inflammaging and Senescence Score, proprietary analytics pipeline. Higher scores denote greater activity of the respective signatures. Additionally, *z*-scores were provided by normalizing these values against a fixed reference population distribution. A 90th percentile (P90) threshold was utilized to designate a sample as an outlier relative to this reference population. Biologically, the Inflammaging Score captures effector and cytokine-driven transcriptional programs, whereas the Senescence Score captures cellular senescence and exhaustion-associated programs.

TCR repertoire analysis. From the clonotype outputs, we derived multiple quantitative metrics to evaluate longitudinal TCR repertoire architecture and dynamics: Repertoire richness (*S*) was defined as the total count of unique clonotypes and normalized across timepoints to reflect overall diversity independent of sequencing depth variations. Repertoire evenness and dominance were quantified using the D_{50} index, representing the minimum percentage of unique clonotypes required to account for 50% of the total sequencing reads. To evaluate structural focus, repertoire clonality was calculated as *1 - Pielou's evenness*, while clonal balance was measured using Shannon equitability (E_H) to reflect the evenness of clonal frequency distributions. To assess clonal space homeostasis, the repertoire was stratified into five fixed frequency size classes based on read fraction: Hyperexpanded (>0.1%), Large (0.01-0.1%), Medium (0.001-0.01%), Small (0.0001-0.001%), and Rare (<0.0001%). Longitudinal repertoire stability and turnover across sampling intervals were quantified as pairwise dissimilarity using *1 - Morisita-Horn index* (%), where lower values indicate higher repertoire stability. One-visit-lag comparisons were used to measure consecutive turnover. The expansion dynamics of dominant clones were tracked over time by computing the cumulative read fraction occupied by the top-5 most-expanded clonotypes at each checkpoint.

T-cell phenotype inference. CD8+ and CD4+ T-cell fractions were inferred from deep TCR-sequencing data (osTCR) using Omniscope's proprietary machine learning models. To evaluate immune system balance, the ratio of CD4+ to CD8+ T-cell fractions was calculated (CD4:CD8 Ratio = CD4 Fraction / CD8 Fraction). For this patient, to quantify phenotypic bias and assess longitudinal deviation from normal physiological bounds, the CD4:CD8 ratio at each timepoint was compared against their healthy baseline timepoint (t0).

Event-related clone calling. For each pair of sampling timepoints anchored to a clinical inflection (onset, t2-t3; emergence of active GO/TED, t6-t7; onset-to-refractory progression, t3-t7; IL-6R blockade, t7-t9), productive TCR clonotypes were compared PRE versus POST on clonotype counts. Each clonotype was tested under the Omniscope Immune Portal (osIP) event-related noise model requiring a ≥2-fold change beyond the noise envelope, with Benjamini–Hochberg control of the false-discovery rate ($q < 0.01$). Clonotypes passing the test were classified as Expanded or Contracted and, orthogonally, as de novo (undetected at PRE time point) or pre-existing (detectable at PRE time point). Per-interval counts of each class are reported in the Results.

Gene-usage enrichment. TRBV and TRBJ segments reported as differentially used across Graves' disease stages were compiled from two high-throughput TCR (CDR3) sequencing studies [Chen 2021; Jia 2022] and grouped into four disjoint disease-stage classes, each segment assigned to exactly one class. General Graves' disease (GD) was defined by TRBV3-2, TRBV7-8, TRBV12-4, TRBV27, TRBV24-1, TRBV11-1, TRBV21-1 and TRBV12-3, together with TRBJ2-4 and TRBJ2-2. Newly diagnosed / early disease (NGD) was defined by TRBV20-1 and TRBV6-9 with TRBJ2-1. Refractory disease (RGD) was defined by TRBV28, TRBV9, TRBV5-5, TRBV7-2, TRBV5-6, TRBV5-8, TRBV6-5 and TRBV14 with TRBJ1-2, TRBJ2-5, TRBJ2-3, TRBJ2-6 and TRBJ1-3. Progression drivers (NGD-RGD) marking the NGD-RGD transition were defined by TRBV15, TRBV4-2, TRBV4-1, TRBV7-9, TRBV6-2, TRBV6-6, TRBV25-1, TRBV10-2 and TRBV10-3 with TRBJ2-7. A clonotype was defined as disease-associated for a class only when both its TRBV and its TRBJ segment belonged to that class; V and J were thus evaluated jointly, in addition to being evaluated independently as single segments. For each interval, the event compartment (expanded, or contracted clonotypes) was then tested against the background of all other, non-mobilized clonotypes in the same pre∪post repertoire. Enrichment was quantified two ways. (i) At the clonotype level, by a one-sided Fisher's exact test on the 2×2 table of disease-associated versus other clonotypes in the event versus background sets, yielding a fold-change and p-value. (ii) At the abundance level, as the count-weighted fold-change of the event compartment relative to background, with significance from a label-permutation null in which the event/background labels were shuffled across clonotypes (1,000 permutations). Both statistics were computed for each single TRBV and TRBJ segment (independent test) and for each stage class as a concrete V∧J set (joint test). Segments and classes were called enriched at fold ≥ 1.5 and $p < 0.05$; event calling used $q < 0.01$ as above.

Gene-level pathway decomposition. We selected the MSigDB hallmark gene set HALLMARK_IL6_JAK_STAT3_SIGNALING (87 genes), 84 of which present in the filtered expression matrix (*CNTFR, INHBE,* and *PLA2G2A* were absent and excluded). To evaluate trajectory shapes independently of expression magnitude, values were standardized per patient across the ten draws into within-patient *z*-scores. Genes with zero variance were excluded. Genes were clustered hierarchically using average linkage on correlation distance to group profiles by trajectory pattern rather than baseline amplitude. The resulting tree was cut into five clusters (correlation distance threshold of 0.90). For visual display, values were clipped to ±2, while underlying *z*-scores remained unclipped. Twelve genes yielded negative corrected CPM values at one or more draws, falling below the anchoring correction floor. These are marked and should be interpreted qualitatively for trajectory ordering rather than exact magnitude.

Statistical analysis. Molecular and clinical trajectories are presented against a common sampling timeline, built from a single shared set of disease-phase intervals and clinical-event annotations so that immune-repertoire, serological and haematological panels are directly co-registered in calendar time across all main and supplementary figures. All analyses and figures were produced in Python 3.13.2 under JupyterLab 4.3.4; specific computational analyses, statistical methods, and algorithm parameters are detailed within the corresponding task descriptions throughout the Methods section.

Glossary

- **Anti-Tg**: Anti-Thyroglobulin Antibodies
- **Anti-TPO**: Anti-Thyroid Peroxidase Antibodies
- **ATA**: American Thyroid Association
- **ATD**: Antithyroid Drug
- **BC**: Breast Cancer
- **BMI**: Body Mass Index
- **CAAR**: Chimeric Autoantibody Receptor
- **CAS**: Clinical Activity Score
- **CRP**: C-Reactive Protein
- **DM**: Diabetes Mellitus
- **DON**: Dysthyroid Optic Neuropathy
- **EUGOGO**: European Group on Graves' Orbitopathy
- **FT3**: Free Triiodothyronine
- **FT4**: Free Thyroxine
- **GD**: Graves' Disease
- **GO**: Graves' Orbitopathy
- **HDL**: High-Density Lipoprotein
- **HLA**: Human Leucocyte Antigen
- **IGF-1R**: Insulin-like Growth Factor 1 Receptor
- **IL-6 / IL-6R**: Interleukin-6 / Interleukin-6 Receptor
- **IOP**: Intra-ocular Pressure
- **IV**: Intravenous
- **LDL**: Low-Density Lipoprotein
- **mAb**: Monoclonal Antibody
- **NGD:** Newly diagnosed Graves' disease
- **NGD-RGD:** Progression drivers of Grave's disease
- **NES**: Normalized Enrichment Score
- **osIP**: Omniscope Immune Portal
- **osTCR:** Omniscope T-Cell Receptor sequencing platform
- **P90:** 90th Percentile threshold
- **PBMC**: Peripheral Blood Mononuclear Cell
- **RA**: Rheumatoid Arthritis
- **RGD:** Refractory Graves' disease
- **RNA**: Ribonucleic Acid
- **RP**: Raynaud's Phenomenon
- **SLK**: Superior Limbic Keratoconjunctivitis
- **STAT3**: Signal Transducer and Activator of Transcription 3
- **TCR:** T-Cell Receptor
- **TED**: Thyroid Eye Disease
- **TNF-α**: Tumor Necrosis Factor alpha
- **TRAb**: TSH Receptor Antibodies
- **TSH**: Thyroid-Stimulating Hormone
- **TSHR**: Thyroid-Stimulating Hormone Receptor
- **TSI**: Thyroid-Stimulating Immunoglobulin
- **WBC**: White Blood Cell Count

Declarations

Ethics and consent. The participant provided written informed consent for the collection and research use of biological samples within the osLifetime programme and for publication of this study and its accompanying clinical data and images. This study adheres to the CARE guidelines for clinical reporting.

Competing interests. A.M.-S., L.J.-G., U.P., M.S., M.G., P.B., J.L.M., M.C., and H.H. are affiliated with Omniscope Inc. R.V.A. serves as a Clinical Advisor for Omniscope Inc., a Medical Doctor at Saint James Hospital Group, and a Longevity Medicine Physician at Elyside Concierge Clinic.

Data availability. Raw sequencing datasets are private due to participant-privacy constraints.

Proprietary components. The osAge model is protected under international patent application (PCT/EP2026/054000).

Acknowledgments. We are deeply thankful to the patient whose cooperation made this study possible, as well as for their consent to publish these details.